Earthquakes and Structures, *Vol. 13, No. 3 (2017) 241-253*
DOI: https://doi.org/10.12989/eas.2017.13.3.241

Earthquake analysis of NFRP-reinforced-concrete beams using hyperbolic shear deformation theory

Sajad Shariati Rad[a] and Mahmood Rabani Bidgoli[*]

Department of Civil Engineering, Jasb Branch, Islamic Azad University, Jasb, Iran

(Received April 11, 2017, Revised September 26, 2017, Accepted September 28, 2017)

Abstract. In this paper, dynamic response of the horizontal nanofiber reinforced polymer (NFRP) strengthened concrete beam subjected to seismic ground excitation is investigated. The concrete beam is modeled using hyperbolic shear deformation beam theory (HSDBT) and the mathematical formulation is applied to determine the governing equations of the structure. Distribution type and agglomeration effects of carbon nanofibers are considered by Mori-Tanaka model. Using the nonlinear strain-displacement relations, stress-strain relations and Hamilton's principle (virtual work method), the governing equations are derived. To obtain the dynamic response of the structure, harmonic differential quadrature method (HDQM) along with Newmark method is applied. The aim of this study is to investigate the effect of NFRP layer, geometrical parameters of beam, volume fraction and agglomeration of nanofibers and boundary conditions on the dynamic response of the structure. The results indicated that applied NFRP layer decreases the maximum dynamic displacement of the structure up to 91 percent. In addition, using nanofibers as reinforcement leads a 35 percent reduction in the maximum dynamic displacement of the structure.

Keywords: dynamic response; NFRP layer; seismic ground excitation; HDQM; Newmark method

1. Introduction

Seismic analysis is a subset of structural analysis in which dynamic response of a building structure (or non-building structures such as bridges, etc.) against the earthquake is examined. This analysis is a part of the structural engineering, the earthquake engineering and seismic retrofitting of the structures which should be constructed in earthquake prone zones.

Liang and Parra-Montesinos (2004) studied seismic behavior of four reinforced concrete column-steel beam under various ground motions using experimental tests. Cheng and Chen (2004) and Changwang *et al.* (2010) studied seismic behavior of steel reinforced concrete column-steel truss beam. They developed a design formula for shear strength of the structure subjected to seismic activities using experimental tests. The effect of cumulative damage on the seismic behavior of steel tube-reinforced concrete (ST-RC) columns through experimental testing was investigated by Ji *et al.* (2014). Six large-scale ST-RC column specimens were subjected to high axial forces and cyclic lateral loading. The effect of plastic hinge relocation on the potential damage of a reinforced concrete frame subjected to different seismic levels was studied by Cao and Ronagh (2014) based on current seismic designs. The optimal seismic retrofit method that uses FRP jackets for shear-critical RC frames was presented by Choi *et al.* (2014). This optimal method uses non-dominated sorting genetic algorithm-II (NSGA-II) to optimize the two conflicting objective functions of the retrofit cost as well as the seismic performance, simultaneously. They examined various parameters like, failure mode, hysteresis curves, ductility and reduction of stiffness. Liu *et al.* (2016) focused on the study of seismic behavior of steel reinforced concrete special-shaped column-beam joints. Six specimens, which are designed according to the principle of strong-member and weak-joint core, are tested under low cyclic reversed load.

In none of the above articles, the nanocomposite structure is considered. Wuite and Adali (2005) performed stress analysis of carbon nanotubes (CNTs) reinforced beams. They concluded that using CNTs as reinforcing phase can increase the stiffness and the stability of the system. Also, Matsunaga (2007) examined stability of the composite cylindrical shell using third-order shear deformation theory (TSDT). Formica *et al.* (2010) analyzed vibration behavior of CNTs reinforced composites. They employed an equivalent continuum model based on Eshelby-Mori-Tanaka model to obtain the material properties of the composite. Liew *et al.* (2014) studied postbuckling of nanocomposite cylindrical panels. They used the extended rule of mixture to estimate the effective material properties of the nanocomposite structure. They also applied a meshless approach to examine the postbuckling response of the nanocomposite cylindrical panel. In another similar work, Lei *et al.* (2014) studied dynamic stability of a CNTs reinforced functionally graded (FG) cylindrical panel. They used Eshelby-Mori-Tanaka model to estimate effective material properties of the resulting nanocomposite structure and also employed Ritz method to distinguish the instability regions of the structure. Static Buckling analysis of CNTs reinforced micro plates is

*Corresponding author, Ph.D.
E-mail: m.rabanibidgoli@gmail.com
[a]Ph.D.

ISSN: 2092-7614 (Print), 2092-7622 (Online)

carried out by Kolahchi *et al.* (2013). They derived the governing equations of the structure based on Mindlin plate theory and using Hamilton's principle. They obtained buckling load of the structure by applying differential quadrature method (DQM). Dynamic response of FG circular cylindrical shells is examined by Davar *et al.* (2013). They developed the mathematical formulation of the structure according to first order shear deformation theory (FSDT) and Love's first approximation theory. Nonlinear vibration of laminated cylindrical shells is analyzed by Shen and Yang (2014). They examined the influences of temperature variation, shell geometric parameter and applied voltage on the linear and nonlinear vibration of the structure. Kolahchi *et al.* (2016) investigated dynamic stability of FG-CNTs reinforced plates. The material properties of the plate are assumed to be a function of temperature and the structure is considered resting on orthotropic elastomeric medium. Jafarian Arani and Kolahchi (2016) presented a mathematical model for buckling analysis of a CNTs reinforced concrete column. They simulated the problem based on Euler Bernoulli and Timoshenko beam theories. Alibeigloo (2016) employed theory of piezo-elasticity to study bending behavior of FG-CNTs reinforced composite cylindrical panels. They used an analytical method to study the effect of CNT volume fraction, temperature variation and applied voltage on the bending behavior of the system. Feng *et al.* (2017a) studied the nonlinear bending behavior of a novel class of multi-layer polymer nanocomposite beams reinforced with graphene platelets (GPLs) that are non-uniformly distributed along the thickness direction. Feng *et al.* (2017b) studied the nonlinear free vibration of a multi-layer polymer nanocomposite beam reinforced by graphene platelets (GPLs) non-uniformly distributed along the thickness direction.

For the first time, dynamic response of NFRP strengthened concrete beams subjected to seismic excitation is studied in the present research. So, the results of this research are of great importance in Civil Engineering. The concrete beam is modeled by applying HSDBT and the effective material properties of the NFRP layer are obtained based on Mori-Tanaka model. The dynamic displacement of structure is calculated by HDQM in conjunction with Newmark method. The effect of nanotechnology on the dynamic response of the structure can be examined by changing the volume fraction of nanofibers in the resulting composite.

2. Mathematical model

In this section, the governing equations of the NFRP strengthened concrete beams are derived by applying HSDBT to analyze the dynamic behavior of the structure.

Fig. 1 illustrates a hollow circular concrete beam subjected to the earthquake loads with outer radius of R_0, inner radius of R_i and thickness of h_c which strengthened by a NFRP layer with thickness of h_f.

By applying HSDBT, the displacements fields are defined as below [21]

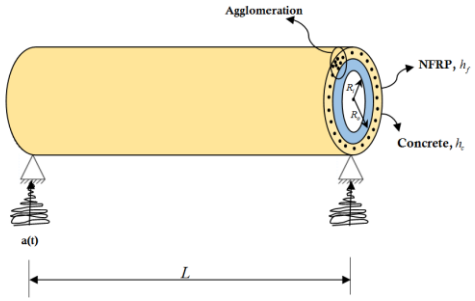

Fig. 1 A schematic figure for concrete columns with NFRP layer under seismic load

$$\begin{aligned} u_1(x,z) &= U(x) - z\frac{\partial W(x)}{\partial x} + \Phi(z)\left(\frac{\partial W(x)}{\partial x} - \phi(x)\right), \\ u_2(x,z) &= 0, \\ u_3(x,z) &= W(x), \end{aligned} \tag{1}$$

where U, V and W are the respective translation displacements of a point at the mid-plane of the beam in the longitudinal x, transverse y and thickness z directions. Also, ϕ denotes the rotation of the cross section area and $\Phi(z)$ is the shape function of the beam which is considered as follows

$$\Phi(z) = h\sinh\left(\frac{z}{h}\right) - z\cosh\left(\frac{1}{2}\right), \tag{2}$$

in which $h = h_f + h_c$. However, the strain-displacement relations of the structure are given as below

$$\begin{aligned} \varepsilon_{xx} &= \left(\frac{\partial U}{\partial x}\right) + \left(\frac{1}{2}\left(\frac{\partial W}{\partial x}\right)^2\right) - z\left(\frac{\partial^2 W}{\partial x^2}\right) \\ &+ \Phi(z)\left(\frac{\partial^2 W}{\partial x^2} - \frac{\partial \varphi}{\partial x}\right), \end{aligned} \tag{3}$$

$$\gamma_{xz} = \frac{\partial \Phi(z)}{\partial z}\left(\frac{\partial W}{\partial x} - \phi\right). \tag{4}$$

The constitutive equations of the orthotropic beam are considered as below

$$\sigma_{xx}^c = C_{11}\varepsilon_{xx}, \tag{5}$$

$$\tau_{xz}^c = C_{44}\gamma_{xz}, \tag{6}$$

Where C_{11} and C_{44} are the elastic constants of the concrete beam. Also, the constitutive equations of the NFRP layer are defined as follows

$$\sigma_{xx}^f = Q_{11}\varepsilon_{xx}, \tag{7}$$

$$\tau_{xz}^f = Q_{44}\gamma_{xz}, \tag{8}$$

in which Q_{11} and Q_{44} are the elastic constants of the NFRP layer. To obtain the effective material properties of the NFRP layer and to consider the agglomeration effect, Mori-

Tanaka model is employed which is introduced in the next section.

3. Mori-Tanaka model

In this section, material properties of resin epoxy polymer reinforced by carbon nanofibers are obtained based on micro-mechanical approach. E_m and ν_m are considered as Young's modulus and Poisson's ratio of the polymer, respectively. The stress-strain relations of the equivalent composite material are given as below [22]

$$\begin{Bmatrix}\sigma_{11}\\ \sigma_{22}\\ \sigma_{33}\\ \sigma_{23}\\ \sigma_{13}\\ \sigma_{12}\end{Bmatrix}=\begin{bmatrix}k+m & l & k-m & 0 & 0 & 0\\ l & n & l & 0 & 0 & 0\\ k-m & l & k+m & 0 & 0 & 0\\ 0 & 0 & 0 & p & 0 & 0\\ 0 & 0 & 0 & 0 & m & 0\\ 0 & 0 & 0 & 0 & 0 & p\end{bmatrix}\begin{Bmatrix}\varepsilon_{11}\\ \varepsilon_{22}\\ \varepsilon_{33}\\ \gamma_{23}\\ \gamma_{13}\\ \gamma_{12}\end{Bmatrix}, \tag{9}$$

where k, l, m, n and p are known as Hill's elastic moduli so that, k is plane-strain bulk modulus normal to the fiber direction, n is the uniaxial tension modulus in the longitudinal direction of the fiber, l is the associated cross modulus, m and p are the shear moduli in planes normal and parallel to the fiber direction, respectively. It should be noted that the mentioned constants depends on the elastic constants of the material. For example, $Q_{11}=k+m$. By applying Mori-Tanaka model, Hill's elastic moduli can be obtained as follows [22]

$$\begin{aligned}
k&=\frac{E_m\{E_m c_m+2k_r(1+\nu_m)[1+c_r(1-2\nu_m)]\}}{2(1+\nu_m)[E_m(1+c_r-2\nu_m)+2c_m k_r(1-\nu_m-2\nu_m^2)]},\\
l&=\frac{E_m\{c_m\nu_m[E_m+2k_r(1+\nu_m)]+2c_r l_r(1-\nu_m^2)]\}}{(1+\nu_m)[E_m(1+c_r-2\nu_m)+2c_m k_r(1-\nu_m-2\nu_m^2)]},\\
n&=\frac{E_m^2 c_m(1+c_r-c_m\nu_m)+2c_m c_r(k_r n_r-l_r^2)(1+\nu_m)^2(1-2\nu_m)}{(1+\nu_m)[E_m(1+c_r-2\nu_m)+2c_m k_r(1-\nu_m-2\nu_m^2)]}\\
&\quad+\frac{E_m[2c_m^2 k_r(1-\nu_m)+c_r n_r(1+c_r-2\nu_m)-4c_m l_r\nu_m]}{E_m(1+c_r-2\nu_m)+2c_m k_r(1-\nu_m-2\nu_m^2)},\\
p&=\frac{E_m[E_m c_m+2p_r(1+\nu_m)(1+c_r)]}{2(1+\nu_m)[E_m(1+c_r)+2c_m p_r(1+\nu_m)]},\\
m&=\frac{E_m[E_m c_m+2m_r(1+\nu_m)(3+c_r-4\nu_m)]}{2(1+\nu_m)\{E_m[c_m+4c_r(1-\nu_m)]+2c_m m_r(3-\nu_m-4\nu_m^2)\}},
\end{aligned} \tag{10}$$

in which k_r, l_r, n_r, p_r and m_r are Hill's elastic moduli of the reinforcing phase of the composite material. Finally by substituting Eq. (10) into Eq. (9), the stiffness matrix can be obtained. The experimental results show that the uniform distribution of the nanofibers is rarely achievable [23]. It is observed that the most of the nanofibers centralized in the regions throughout the matrix. These regions are assumed to be in spherical shapes which known as "inclusions" with different material properties from the surrounding regions. V_r is the total volume of nanofibers and is defined as

$$V_r=V_r^{inclusion}+V_r^m, \tag{11}$$

in which $V_r^{inclusion}$ and V_r^m represent the volume of the CNTs inside the inclusion and polymer matrix, respectively. The agglomeration effect can be considered based on the micro-mechanical model by introducing the two following parameters

$$\xi=\frac{V_{inclusion}}{V}, \tag{12}$$

$$\zeta=\frac{V_r^{inclusion}}{V_r}. \tag{13}$$

The average volume fraction C_r of nanofibers in the composite material is given as follows

$$C_r=\frac{V_r}{V}. \tag{14}$$

The volume fraction of nanofibers inside the inclusion and the matrix (concrete) can be defined as

$$\frac{V_r^{inclusion}}{V_{inclusion}}=\frac{C_r\zeta}{\xi}, \tag{15}$$

$$\frac{V_r^m}{V-V_{inclusion}}=\frac{C_r(1-\zeta)}{1-\xi}. \tag{16}$$

We assume that nanofibers are transversely isotropic and the orientation of them is randomly. Hence, the inclusion is considered to be isotropic and the effective bulk modulus K and shear modulus G may be written as below

$$K=K_{out}\left[1+\frac{\xi\left(\frac{K_{in}}{K_{out}}-1\right)}{1+\alpha(1-\xi)\left(\frac{K_{in}}{K_{out}}-1\right)}\right], \tag{17}$$

$$G=G_{out}\left[1+\frac{\xi\left(\frac{G_{in}}{G_{out}}-1\right)}{1+\beta(1-\xi)\left(\frac{G_{in}}{G_{out}}-1\right)}\right], \tag{18}$$

in which K_{in} and K_{out} are the effective bulk modulus of the inclusion and the matrix outside the inclusion, respectively. Also, G_{in} and G_{out} are the effective shear modulus of the inclusion and the matrix outside the inclusion, respectively and are given as follows

$$K_{in}=K_m+\frac{(\delta_r-3K_m\chi_r)C_r\zeta}{3(\xi-C_r\zeta+C_r\zeta\chi_r)}, \tag{19}$$

$$K_{out}=K_m+\frac{C_r(\delta_r-3K_m\chi_r)(1-\zeta)}{3[1-\xi-C_r(1-\zeta)+C_r\chi_r(1-\zeta)]}, \tag{20}$$

$$G_{in} = G_m + \frac{(\eta_r - 3G_m\beta_r)C_r\zeta}{2(\xi - C_r\zeta + C_r\zeta\beta_r)}, \tag{21}$$

$$G_{out} = G_m + \frac{C_r(\eta_r - 3G_m\beta_r)(1-\zeta)}{2\left[1-\xi - C_r(1-\zeta) + C_r\beta_r(1-\zeta)\right]}, \tag{22}$$

where $\chi_r, \beta_r, \delta_r$ and η_r can be obtained as

$$\chi_r = \frac{3(K_m + G_m) + k_r - l_r}{3(k_r + G_m)}, \tag{23}$$

$$\beta_r = \frac{1}{5}\left\{\begin{array}{l}\dfrac{4G_m + 2k_r + l_r}{3(k_r + G_m)} + \dfrac{4G_m}{(p_r + G_m)} \\ + \dfrac{2\left[G_m(3K_m + G_m) + G_m(3K_m + 7G_m)\right]}{G_m(3K_m + G_m) + m_r(3K_m + 7G_m)}\end{array}\right\}, \tag{24}$$

$$\delta_r = \frac{1}{3}\left[n_r + 2l_r + \frac{(2k_r - l_r)(3K_m + 2G_m - l_r)}{k_r + G_m}\right], \tag{25}$$

$$\eta_r = \frac{1}{5}\left[\begin{array}{l}\dfrac{2}{3}(n_r - l_r) + \dfrac{8G_m m_r(3K_m + 4G_m)}{3K_m(m_r + G_m) + G_m(7m_r + G_m)} \\ + \dfrac{2(k_r - l_r)(2G_m + l_r)}{3(k_r + G_m)} + \dfrac{4G_m p_r}{(p_r + G_m)}\end{array}\right], \tag{26}$$

K_m and G_m are the bulk and shear moduli of the matrix phase which are defined as below

$$K_m = \frac{E_m}{3(1-2\upsilon_m)}, \tag{27}$$

$$G_m = \frac{E_m}{2(1+\upsilon_m)}. \tag{28}$$

Moreover, α and β in Eqs. (17) and (18) are given as follows

$$\alpha = \frac{(1+\upsilon_{out})}{3(1-\upsilon_{out})}, \tag{29}$$

$$\alpha = \frac{(1+\upsilon_{out})}{3(1-\upsilon_{out})}, \tag{30}$$

$$\upsilon_{out} = \frac{3K_{out} - 2G_{out}}{6K_{out} + 2G_{out}}. \tag{31}$$

Therefore, the effective Young's modulus E and Poisson's ratio v of the composite material are given by

$$E = \frac{9KG}{3K + G}, \tag{32}$$

$$\upsilon = \frac{3K - 2G}{6K + 2G}. \tag{33}$$

4. Energy method

To derive the governing equations of the structure by employing energy method and using Hamilton's principle, the work done by external forces is equated to the strain energy and kinetic energy stored in the structure. The potential strain energy stored in the structure is given as follows

$$\begin{aligned} U &= \int_{V_c}\left(\sigma_{xx}^c\varepsilon_{xx} + \tau_{xz}^c\gamma_{xz}\right)dA_c dx \\ &+ \int_{V_f}\left(\sigma_{xx}^f\varepsilon_{xx} + \tau_{xz}^f\gamma_{xz}\right)dA_f dx, \end{aligned} \tag{34}$$

where A_c and A_f are the cross section area of the concrete beam and NFRP layer, respectively. By substituting Eqs. (3) and (4) into Eq. (34) we have

$$\begin{aligned} U &= \frac{1}{2}\int_0^L\left[\int_{A_c}\left[\sigma_{xx}^c\left\{\left(\frac{\partial U}{\partial x}\right) + \left(\frac{1}{2}\left(\frac{\partial W}{\partial x}\right)^2\right) - z\left(\frac{\partial^2 W}{\partial x^2}\right)\right.\right.\right. \\ &\left.\left.\left. + \Phi(z)\left(\frac{\partial^2 W}{\partial x^2} - \frac{\partial\varphi}{\partial x}\right)\right\} + \tau_{xz}^c\left\{\frac{\partial\Phi(z)}{\partial z}\left(\frac{\partial W}{\partial x} - \varphi\right)\right\}\right]dA_c dx \\ &+ \frac{1}{2}\int_0^L\left[\int_{A_f}\left[\sigma_{xx}^f\left\{\left(\frac{\partial U}{\partial x}\right) + \left(\frac{1}{2}\left(\frac{\partial W}{\partial x}\right)^2\right) - z\left(\frac{\partial^2 W}{\partial x^2}\right)\right.\right.\right. \\ &\left.\left.\left. + \Phi(z)\left(\frac{\partial^2 W}{\partial x^2} - \frac{\partial\varphi}{\partial x}\right)\right\} + \tau_{xz}^f\left\{\frac{\partial\Phi(z)}{\partial z}\left(\frac{\partial W}{\partial x} - \varphi\right)\right\}\right]dA_f dx. \end{aligned} \tag{35}$$

By defining the in-plane stress resultants as follows

$$N_x = \int_{A_c}\sigma_{xx}^c dA_c + \int_{A_f}\sigma_{xx}^f dA_f, \tag{36}$$

$$M_x = \int_{A_c}\sigma_{xx}^c z dA_c + \int_{A_f}\sigma_{xx}^f z dA_f, \tag{37}$$

$$F_x = \int_{A_c}\sigma_{xx}^c\Phi(z) dA_c + \int_{A_f}\sigma_{xx}^f\Phi(z) dA_f, \tag{38}$$

$$Q_x = \int_{A_c}\tau_{xz}^c\frac{\partial\Phi(z)}{\partial z}dA_c + \int_{A_f}\tau_{xz}^f\frac{\partial\Phi(z)}{\partial z}dA_f, \tag{39}$$

Eq. (35) can be rewritten as below

$$\begin{aligned} U = \frac{1}{2}\int_0^L\left[\int\left[N_x\left(\left(\frac{\partial U}{\partial x}\right) + \left(\frac{1}{2}\left(\frac{\partial W}{\partial x}\right)^2\right)\right) - M_x\left(\frac{\partial^2 W}{\partial x^2}\right)\right.\right. \\ \left.\left. + F_x\left(\frac{\partial^2 W}{\partial x^2} - \frac{\partial\phi}{\partial x}\right) + Q_x\left(\left(\frac{\partial W}{\partial x} - \phi\right)\right)\right]dx, \end{aligned} \tag{40}$$

By substituting Eqs. (5)-(8) into Eqs. (36)-(39), the stress resultants of the beam take the following form

$$N_x = A_{11}\left(\frac{\partial U}{\partial x}+\frac{1}{2}\left(\frac{\partial W}{\partial x}\right)^2\right)-B_{11}\left(\frac{\partial^2 W}{\partial x^2}\right) +E_{11}\left(\frac{\partial^2 W}{\partial x^2}-\frac{\partial \varphi}{\partial x}\right), \tag{41}$$

$$M_x = B_{11}\left(\frac{\partial U}{\partial x}+\frac{1}{2}\left(\frac{\partial W}{\partial x}\right)^2\right)-D_{11}\left(\frac{\partial^2 W}{\partial x^2}\right) +F_{11}\left(\frac{\partial^2 W}{\partial x^2}-\frac{\partial \varphi}{\partial x}\right), \tag{42}$$

$$F_x = E_{11}\left(\frac{\partial U}{\partial x}+\frac{1}{2}\left(\frac{\partial W}{\partial x}\right)^2\right)-F_{11}\left(\frac{\partial^2 W}{\partial x^2}\right) +H_{11}\left(\frac{\partial^2 W}{\partial x^2}-\frac{\partial \varphi}{\partial x}\right), \tag{43}$$

$$Q_x = L_{44}\left(\frac{\partial W}{\partial x}-\phi\right), \tag{44}$$

in which

$$A_{11}=\int_{A_c} C_{11}\,dA_c+\int_{A_f} Q_{11}\,dA_f, \tag{45}$$

$$B_{11}=\int_{A_c} C_{11}\,z dA_c+\int_{A_f} Q_{11}\,z dA_f, \tag{46}$$

$$D_{11}=\int_{A_c} C_{11}\,z^2 dA_c+\int_{A_f} Q_{11}\,z^2 dA_f, \tag{47}$$

$$E_{11}=\int_{A_c} C_{11}\,\Phi(z) dA_c+\int_{A_f} Q_{11}\,\Phi(z) dA_f, \tag{48}$$

$$F_{11}=\int_{A_c} C_{11}\,z\Phi(z) dA_c+\int_{A_f} Q_{11}\,z\Phi(z) dA_f, \tag{49}$$

$$H_{11}=\int_{A_c} C_{11}\,\Phi(z)^2 dA_c+\int_{A_f} Q_{11}\,\Phi(z)^2 dA_f, \tag{50}$$

$$L_{44}=\int_{A_c} C_{11}\frac{\partial\Phi(z)}{\partial z} dA_c+\int_{A_f} Q_{11}\frac{\partial\Phi(z)}{\partial z} dA_f. \tag{51}$$

The kinetic energy of the structure are defined as below

$$K=\frac{\rho}{2}\int\left(\dot{u}_1^{\,2}+\dot{u}_2^{\,2}+\dot{u}_3^{\,2}\right)dV \tag{52}$$

By substituting Eq. (1) into Eq. (52) we have

$$K=\frac{\rho}{2}\int\left(\left(\frac{\partial U}{\partial t}-z\frac{\partial^2 W}{\partial x\partial t}+\Phi(z)\left(\frac{\partial^2 W}{\partial x\partial t}-\frac{\partial\phi}{\partial t}\right)\right)^2+\left(\frac{\partial W}{\partial t}\right)^2\right)dV. \tag{53}$$

By defining the inertia moment terms as

$$\begin{Bmatrix} I_0\\ I_1\\ I_2\\ I_3\\ I_4\\ I_5\end{Bmatrix}=\int_{A_c}\begin{bmatrix}\rho_c\\ \rho_c z\\ \rho_c z^2\\ \rho_c\Phi(z)\\ \rho_c z\Phi(z)\\ \rho_c\Phi(z)^2\end{bmatrix}dA_c+\int_{A_f}\begin{bmatrix}\rho_f\\ \rho_f z\\ \rho_f z^2\\ \rho_f\Phi(z)\\ \rho_f z\Phi(z)\\ \rho_f\Phi(z)^2\end{bmatrix}dA_f, \tag{54}$$

Eq. (53) can be rewritten as below

$$K=0.5\int\left[I_0\left(\left(\frac{\partial U}{\partial t}\right)^2+\left(\frac{\partial W}{\partial t}\right)^2\right)-2I_1\left(\frac{\partial U}{\partial t}\frac{\partial^2 W}{\partial x\,\partial t}\right) +I_2\left(\frac{\partial^2 W}{\partial x\,\partial t}\right)^2+I_3\frac{\partial U}{\partial t}\left(\frac{\partial^2 W}{\partial x\,\partial t}-\frac{\partial\varphi}{\partial t}\right) -I_4\frac{\partial^2 W}{\partial x\,\partial t}\left(\frac{\partial^2 W}{\partial x\,\partial t}-\frac{\partial\varphi}{\partial t}\right)+I_5\left(\frac{\partial^2 W}{\partial x\,\partial t}-\frac{\partial\varphi}{\partial t}\right)^2\right]dx. \tag{55}$$

The external work due the earthquake can be calculated as follows

$$W=\int\underbrace{(ma(t))}_{F_{Seismic}}Wdx, \tag{56}$$

where m and $a(t)$ are the mass and acceleration of the earth, respectively. To extract the governing equations of motion, Hamilton's principle is expressed as follows [24, 25]

$$\int_0^t(\delta U-\delta K-\delta W)dt=0, \tag{57}$$

Where δ denotes the variational operator. By considering Eqs. (40), (55) and (56), the first variations of the potential strain energy, the kinetic energy and the external work are presented as below

$$\delta U=\int_0^L\left[\int\left[N_x\left(\frac{\partial\delta U}{\partial x}+\frac{\partial W}{\partial x}\frac{\partial\delta W}{\partial x}\right)-M_x\left(\frac{\partial^2\delta W}{\partial x^2}\right) +F_x\left(\frac{\partial^2\delta W}{\partial x^2}-\frac{\partial\delta\phi}{\partial x}\right)+Q_x\left(\left(\frac{\partial\delta W}{\partial x}-\delta\phi\right)\right)\right]dx, \tag{58}$$

$$\delta K=\int_0^L\left[I_0\left(\frac{\partial U}{\partial t}\frac{\partial\delta U}{\partial t}+\frac{\partial W}{\partial t}\frac{\partial\delta W}{\partial t}\right) -I_1\left(\frac{\partial\delta U}{\partial t}\frac{\partial^2 W}{\partial x\,\partial t}+\frac{\partial U}{\partial t}\frac{\partial^2\delta W}{\partial x\,\partial t}\right)+I_2\left(\frac{\partial^2 W}{\partial x\,\partial t}\frac{\partial^2\delta W}{\partial x\,\partial t}\right) +I_3\left(\frac{\partial\delta U}{\partial t}\left(\frac{\partial^2 W}{\partial x\,\partial t}-\frac{\partial\varphi}{\partial t}\right)+\frac{\partial U}{\partial t}\left(\frac{\partial^2\delta W}{\partial x\,\partial t}-\frac{\partial\delta\varphi}{\partial t}\right)\right) -I_4\left(\frac{\partial^2\delta W}{\partial x\,\partial t}\left(\frac{\partial^2 W}{\partial x\,\partial t}-\frac{\partial\varphi}{\partial t}\right)+\frac{\partial^2 W}{\partial x\,\partial t}\left(\frac{\partial^2\delta W}{\partial x\,\partial t}-\frac{\partial\delta\varphi}{\partial t}\right)\right) +I_5\left(\frac{\partial^2 W}{\partial x\,\partial t}-\frac{\partial\varphi}{\partial t}\right)\left(\frac{\partial^2\delta W}{\partial x\,\partial t}-\frac{\partial\delta\varphi}{\partial t}\right)\right]dx, \tag{59}$$

$$\delta W = -\int (\underbrace{ma(t)}_{F_{Seismic}})\delta W dx, \tag{60}$$

Now, by substituting Eqs. (58)-(60) into Eq. (57), the motion equations of the structure are obtained as follows

δU :

$$\frac{\partial N_x}{\partial x} = I_0 \frac{\partial^2 U}{\partial t^2} + (I_3 - I_1)\frac{\partial^3 W}{\partial x \partial t^2} - I_3 \frac{\partial^2 \varphi}{\partial t^2}, \tag{61}$$

δW :

$$\begin{aligned} &\frac{\partial^2 M_x}{\partial x^2} - \frac{\partial}{\partial x}\left(N_x^M \frac{\partial W}{\partial x}\right) - \frac{\partial^2 F_x}{\partial x^2} + \frac{\partial Q_x}{\partial x} + F_{Seismic} \\ &= I_0 \frac{\partial^3 W}{\partial t^2} + (I_1 - I_3)\frac{\partial^3 U}{\partial x \partial t^2} \\ &+ (2I_4 - I_2 - I_5)\frac{\partial^4 W}{\partial x^2 \partial t^2} + (I_5 - I_4)\frac{\partial^3 \varphi}{\partial x \partial t^2}, \end{aligned} \tag{62}$$

$\delta \varphi$:

$$Q_x - \frac{\partial F_x}{\partial x} = I_5 \frac{\partial^2 \varphi}{\partial t^2} - I_3 \frac{\partial^2 U}{\partial t^2} + (I_4 - I_5)\frac{\partial^3 W}{\partial x \partial t^2}, \tag{63}$$

By substituting Eqs. (41)-(44) into Eqs. (61)-(63), the governing equations of the system are expressed as follows

$$\begin{aligned} &\delta U : A_{11}\left(\frac{\partial^2 U}{\partial x^2} + \frac{\partial W}{\partial x}\frac{\partial^2 W}{\partial x^2}\right) - B_{11}\left(\frac{\partial^3 W}{\partial x^3}\right) \\ &+ E_{11}\left(\frac{\partial^3 W}{\partial x^3} - \frac{\partial^2 \varphi}{\partial x^2}\right) = I_0 \frac{\partial^2 U}{\partial t^2} \\ &+ (I_3 - I_1)\frac{\partial^3 W}{\partial x \partial t^2} - I_3 \frac{\partial^2 \varphi}{\partial t^2}, \end{aligned} \tag{64}$$

$$\begin{aligned} &\delta W : (B_{11} - E_{11})\left(\frac{\partial^3 U}{\partial x^3} + \left(\frac{\partial^2 W}{\partial x^2}\right)^2 + \frac{\partial W}{\partial x}\frac{\partial^3 W}{\partial x^3}\right) \\ &- (D_{11} - F_{11})\left(\frac{\partial^4 W}{\partial x^4}\right) + (F_{11} - H_{11})\left(\frac{\partial^4 W}{\partial x^4} - \frac{\partial^3 \varphi}{\partial x^3}\right) \\ &+ L_{44}\left(\frac{\partial^2 W}{\partial x^2} - \frac{\partial \varphi}{\partial x}\right) + F_{Seismic} = I_0 \frac{\partial^2 W}{\partial t^2} + (I_1 - I_3)\frac{\partial^3 U}{\partial x \partial t^2} \\ &+ (2I_4 - I_2 - I_5)\frac{\partial^4 W}{\partial x^2 \partial t^2} + (I_5 - I_4)\frac{\partial^3 \varphi}{\partial x \partial t^2}, \end{aligned} \tag{65}$$

$$\begin{aligned} &\delta \varphi : Q_x - E_{11}\left(\frac{\partial^2 U}{\partial x^2} + \frac{\partial W}{\partial x}\frac{\partial^2 W}{\partial x^2}\right) + F_{11}\left(\frac{\partial^{33} W}{\partial x^3}\right) \\ &- H_{11}\left(\frac{\partial^3 W}{\partial x^3} - \frac{\partial^2 \varphi}{\partial x^2}\right) = I_5 \frac{\partial^2 \varphi}{\partial t^2} - I_3 \frac{\partial^2 U}{\partial t^2} \\ &+ (I_4 - I_5)\frac{\partial^3 W}{\partial x \partial t^2}, \end{aligned} \tag{66}$$

Also, the boundary conditions of the structure are considered as below

• Clamped-Clamped supported

$$\begin{aligned} &W = U = \phi = \frac{\partial W}{\partial x} = 0, && @ \quad x = 0 \\ &W = U = \phi = \frac{\partial W}{\partial x} = 0. && @ \quad x = L \end{aligned} \tag{67}$$

•Clamped-Simply supported

$$\begin{aligned} &W = U = \phi = \frac{\partial W}{\partial x} = 0, && @ \quad x = 0 \\ &W = U = \phi = M_x = 0. && @ \quad x = L \end{aligned} \tag{68}$$

•Simply-Simply supported

$$\begin{aligned} &W = U = \phi = M_x = 0, && @ \quad x = 0 \\ &W = U = \phi = M_x = 0. && @ \quad x = L \end{aligned} \tag{69}$$

•Clamped-Free

$$\begin{aligned} &W = U = \phi = \frac{\partial W}{\partial x} = 0, && @ \quad x = 0 \\ &F_x = Q_x = N_x = M_x = 0. && @ \quad x = L \end{aligned} \tag{70}$$

5. Solution procedure

In this study, HDQM is applied to examine the dynamic behavior of the structure. In this numerical method, the governing differential equations of the structure turn into a set of first order algebraic equations by applying the weighting coefficients. According to HDQ method, a derivative of a function at a given discrete point will be approximated as a weighted linear sum of the function values at all discrete points chosen in the solution domain. The one-dimensional derivative of the function can be expressed as follows [26]

$$\frac{d^n f(x_i)}{dx^n} = \sum_{j=1}^{N} C_{ij}^{(n)} f(x_j) \qquad n = 1,...,N-1. \tag{71}$$

Where $f(x)$ is the mentioned function, N denotes number of grid points, x_i is a sample point of the function domain, f_i is the value of the function at ith sample point and C_{ij} indicates the weighting coefficients. So, choosing the grid points and weighting coefficients is an important factor in the accuracy of the results. The grid points are considered by Chebyshev polynomials as follows

$$X_i = \frac{L}{2}\left[1 - \cos\left(\frac{i-1}{N_x - 1}\right)\pi\right] \quad i = 1,...,N_x \tag{72}$$

Based on Chebyshev polynomials, the grid points are closer together near the borders and in distant parts of the borders they away from each other. The weighting coefficients may be calculated by the following simple algebraic relations

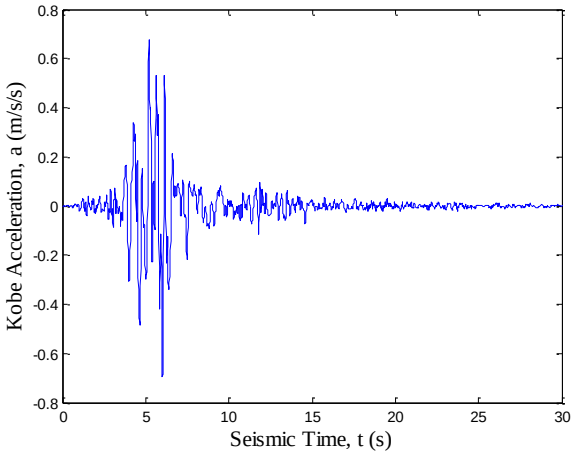

Fig. 2 Acceleration history of Kobe earthquake

$$A_{ij}^{(1)}=\begin{cases}\dfrac{(\pi/2)M(x_i)}{M(x_j)\sin[(x_i-x_j)/2]\pi} & for \quad i\neq j, \quad i,j=1,2,...,N_x,\\ -\sum\limits_{\substack{j=1\\ i\neq j}}^{N_x}A_{ij}^{(1)} & for \quad i=j, \quad i,j=1,2,...,N_x\end{cases} \tag{73}$$

in which

$$M(x_i)=\prod_{\substack{j=1\\ j\neq i}}^{N_x}\sin\left(\frac{(x_i-x_j)\pi}{2}\right) \tag{74}$$

Also, the higher-order derivatives are considered as

$$A_{ij}^{(n)}=n\left(A_{ii}^{(n-1)}A_{ij}^{(1)}-\pi ctg\left(\frac{x_i-x_j}{2}\right)\pi\right) \tag{75}$$

By distributing the grid points in the domain based on Eq. (72) and by substituting Eq. (71) into the governing equations, we have

$$\left(\left[\underbrace{K_L+K_{NL}}_{K}\right]\begin{Bmatrix}\{d_b\}\\ \{d_d\}\end{Bmatrix}+[M]\begin{Bmatrix}\{\ddot{d}_b\}\\ \{\ddot{d}_d\}\end{Bmatrix}\right)=\begin{Bmatrix}\{0\}\\ -Ma(t)\end{Bmatrix}, \tag{76}$$

in which $[K_L]$, $[K_{NL}]$ and $[M]$ indicate linear part of the stiffness matrix, nonlinear part of the stiffness matrix and the mass matrix, respectively. Also, $\{d_b\}$ and $\{d_d\}$ denote boundary and domain points, respectively. To obtain the time response of the structure subjected to the earthquake loads Newmark method [27] is applied in the time domain. Based on this method, Eq. (76) is considered in the general form as below

$$K^*(d_{i+1})=Q_{i+1}, \tag{77}$$

where subscript i+1denotes the time $t=t_{i+1}$, $K^*(d_{i+1})$ and Q_{i+1} are the effective stiffness matrix and the effective load vector which are given as

$$K^*(d_{i+1})=K_L+K_{NL}(d_{i+1})+\alpha_0 M+\alpha_1 C, \tag{78}$$

$$\begin{aligned}Q_{i+1}^*&=Q_{i+1}+M\left(\alpha_0 d_i+\alpha_2\dot{d}_i+\alpha_3\ddot{d}_i\right)\\ &+C\left(\alpha_1 d_i+\alpha_4\dot{d}_i+\alpha_5\ddot{d}_i\right),\end{aligned} \tag{79}$$

where [27]

$$\begin{aligned}&\alpha_0=\frac{1}{\chi\Delta t^2}, \quad \alpha_1=\frac{\gamma}{\chi\Delta t}, \quad \alpha_2=\frac{1}{\chi\Delta t},\\ &\alpha_3=\frac{1}{2\chi}-1, \quad \alpha_4=\frac{\gamma}{\chi}-1, \alpha_5=\frac{\Delta t}{2}\left(\frac{\gamma}{\chi}-2\right), \ ,\\ &\alpha_6=\Delta t\,(1-\gamma), \quad \alpha_7=\Delta t\,\gamma,\end{aligned} \tag{80}$$

where γ=0.5 and χ=0.25. By applying the iteration method, Eq. (77) is solved at any time step and modified velocity and acceleration vectors are computed as follows

$$\ddot{d}_{i+1}=\alpha_0(d_{i+1}-d_i)-\alpha_2\dot{d}_i-\alpha_3\ddot{d}_i, \tag{81}$$

$$\dot{d}_{i+1}=\dot{d}_i+\alpha_6\ddot{d}_i+\alpha_7\ddot{d}_{i+1}, \tag{82}$$

Then for the next time step, the modified velocity and acceleration vectors in Eqs. (81) and (82) are applied and all the mentioned procedures are repeated.

6. Numerical results

In this section, the effect of various parameters on the dynamic response of the NFRP strengthened concrete beam under seismic load is examined. The outer radius and the inner radius of the concrete beam are R_0= 205 mm and R_i=56 mm, respectively and the length of the beam is L=3 m. The elastic moduli of concrete, epoxy resin and carbon nanofiber are E_c=20 GPa, Ef=25 GPa and E_r=1 TPa, respectively. In this study, the influences of NFRP layer, carbon nanofiber volume fraction, geometric parameters and boundary conditions on the dynamic displacement of the structure are investigated. The earthquake acceleration is considered based on Kobe earthquake that the distribution of acceleration in 30 seconds is shown in Fig. 2.

6.1 Convergence of HDQM

Figs. 3(a)-(d) shows the convergence of HDQM in evaluating the maximum deflection of the structure versus time.

As it can be seen, with increasing the number of grid points N, the maximum deflection of the structure decreases. For example, the maximum deflections of the structure for the number of grid points (N) of 7, 11, 15 and 17 are equal to 0.14, 0.06, 0.016 and 0015, respectively. It can be found that by increasing the number of grid points, the decay ratio of the dynamic deflection decreases as far as at N=17 the dynamic deflection converges. It means that the increasing of the number of grid points does not affect the amount of the dynamic displacement of the structure after N=17. So, the results presented below are based on the number of grid points 17 for HDQ solution method.

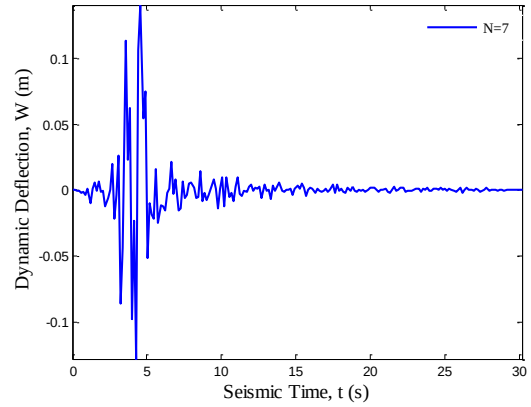

(a)

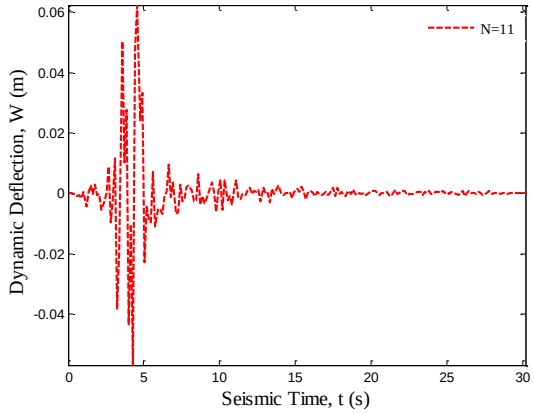

(b)

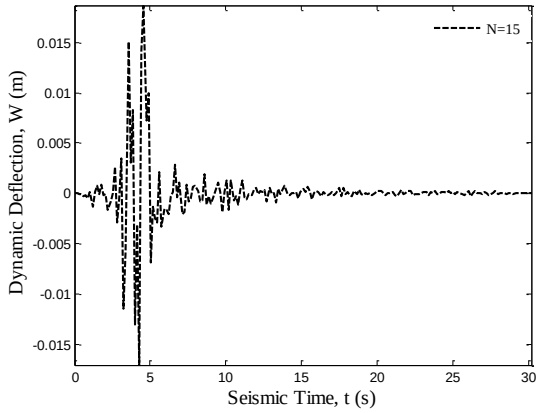

(c)

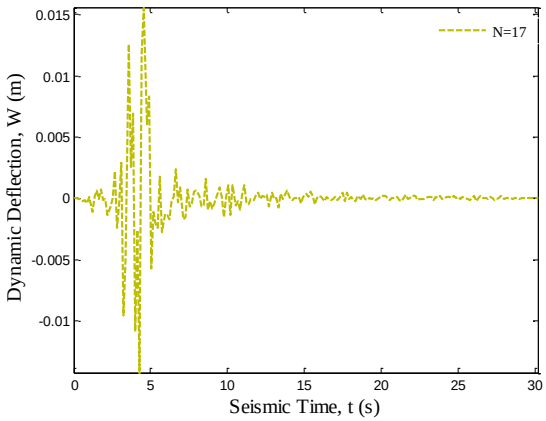

(d)

Fig. 3 Convergence and accuracy of HDQM

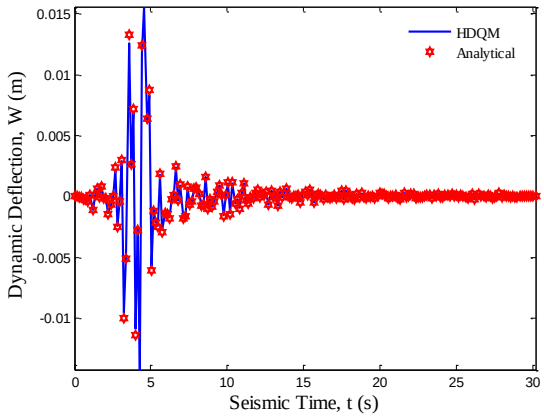

Fig. 4 Comparison of analytical and numerical results

6.2 Validation of results

Given that no similar work has been done to validate the present study, so, it has been tried to examine the results without considering the nonlinear terms of the governing equations and by comparing the linear dynamic response of the structure which obtained by two various solution methods. The results of the analytical and numerical (HDQ) methods are depicted in Fig. 4. As it can be observed, the results of numerical and analytical methods are identical and therefore, the obtained results are accurate and acceptable.

6.3 Effect of NFRP layer on the dynamic response

Figs. 5 (a)-(d) illustrate the effect of NFRP layer on the dynamic deflection versus time and various thicknesses of the NFRP layer.

As it can be observed, the structure without NFRP layer has a greater dynamic deflection with respect to the concrete beam covered with a NFRP layer. The reason is that the NFRP layer increases the stiffness of the structure. Fig. 5(a) shows the maximum dynamic deflection of the structure without NFRP layer equal to 0.059 while by applying the NFRP layer with thicknesses of 30, 60 and 90 mm, the maximum dynamic displacement of the structure is 0.0207, 0.0053 and 0.0045, respectively. By comparing the results, we can say that using the NFRP layer with thicknesses of 30, 60 and 90 mm decreases the maximum dynamic displacement of the structure up to 64.9, 91.02 and 92.37% which is a remarkable result in the dynamic designing of the structures. Also it should be noted that the excessive increasing of the NFRP layer (hf>60 mm) increases costs while it does not have a noticeable effect on
the dynamic response of the structure. Hence, the NFRP layer with thickness of 60 mm is the best choice for the present structure.

6.4 Effect of carbon nanofibers on the dynamic response

As mentioned in the previous sections, the NFRP is reinforced by carbon nanofibers instead of macro fibers. In

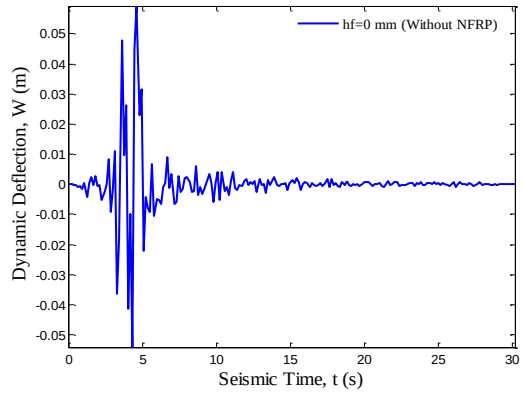

(a)

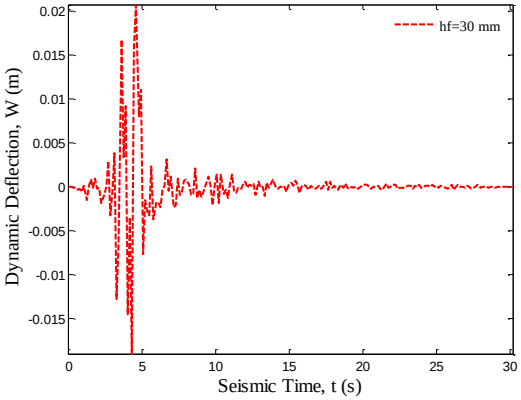

(b)

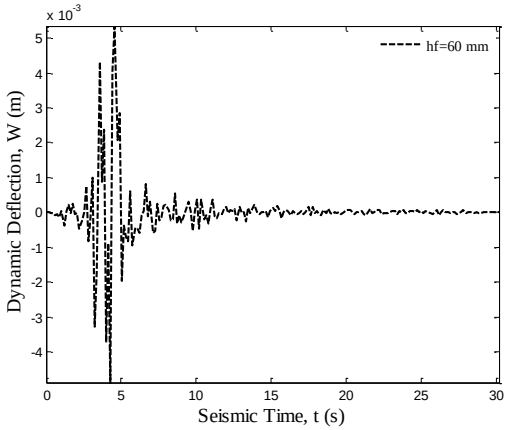

(c)

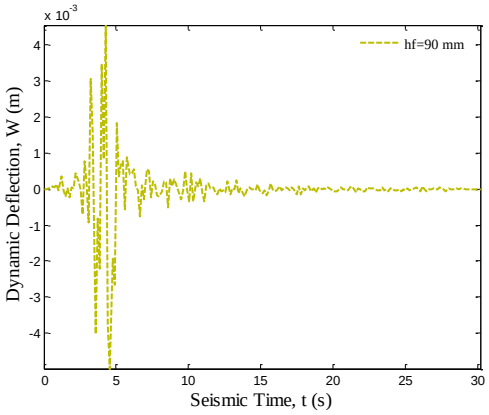

(d)

Fig. 5 The effect of NFRP layer on the dynamic deflection of the structure

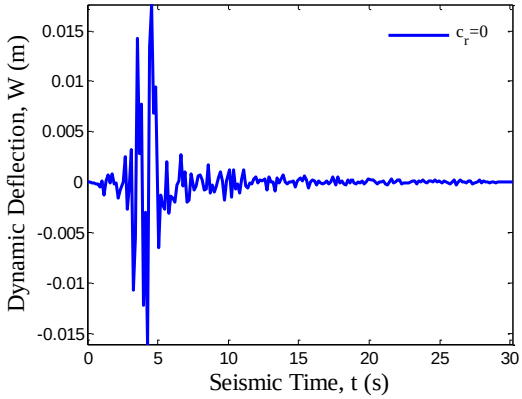

(a)

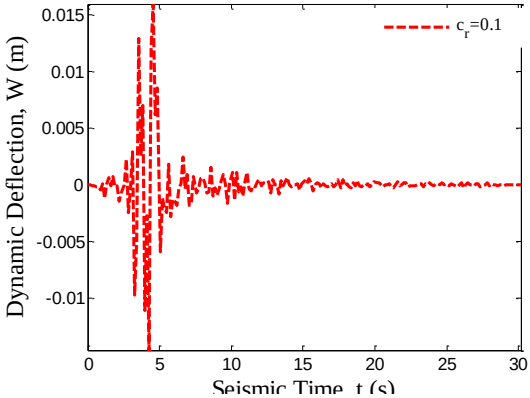

(b)

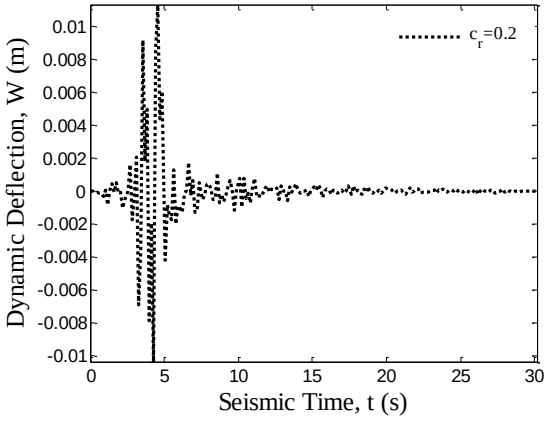

(c)

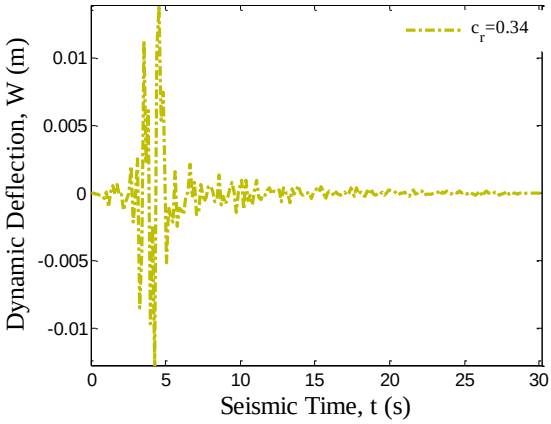

(d)

Fig. 6 The effect of nanofibers volume percent on the dynamic deflection of the structure

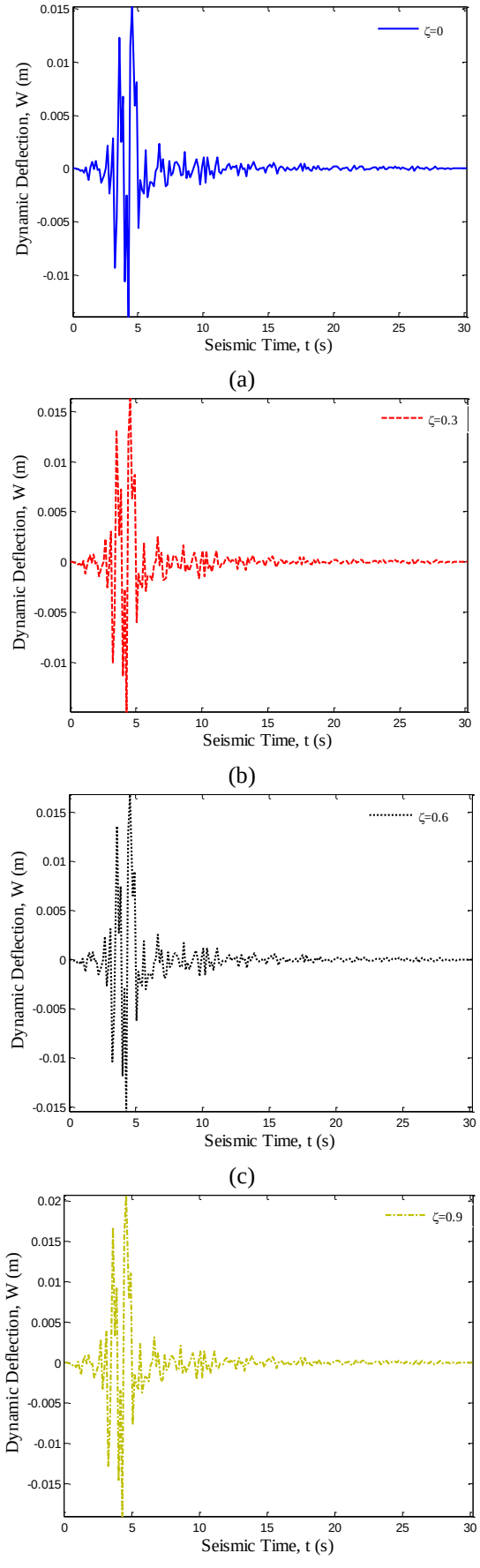

Fig. 7 The effect of nanofibers agglomeration on the dynamic deflection of the structure

this section, the effect of nanofibers volume percent on the dynamic response of the structure is studied.

Figs. 6(a)-(d) shows the dynamic deflection of the structure versus time for different values of nanofibers volume fraction as c_r=0, c_r=0.1, c_r=0.2 and c_r=0.34, respectively. It is apparent that the maximum dynamic displacement of the structure is equals to 0.0176 for the case of c_r=0 (without nanofibers). By applying nanofibers with volume fractions of 0.1, 0.2 and 0.34, the amount of maximum dynamic displacement is 0.0159, 0.0113 and 0.0139, respectively. Therefore, using nanofibers with volume fractions of 0.1 and 0.2 increases the stiffness of the structure and reduces the maximum displacement of structure 9.65 and 35.79 percent, respectively.

It is also worth to mention that the volume percent of 0.34 is an optimum value since before 0.34 percent, the deflection is decreased while for after 0.34 percent, the deflection increases. So it can be concluded that with increasing the volume fraction of nanofibers, the dynamic deflection of the system decreases and it is because of the increasing of the stiffness of the structure.

The agglomeration effect of nanofibers on the dynamic deflection of the structure versus time is illustrated in Figs. 7(a)-(d). As it can be observed, by considering the agglomeration effect, the stiffness of the structure reduces while the dynamic displacement increases. For example, in the absence of the agglomeration effect (ξ=0), the maximum dynamic deflection of the structure is 0.0152 while for ξ=0.9 the maximum dynamic deflection is 0.0207.

The results reveal that the existence of the agglomeration changes the maximum dynamic displacement of the structure up to 36.18%. Since during the process of nanocomposite manufacturing, the uniform distribution for nanofibers in the matrix is impossible, so the results of this figure can be very remarkable.

6.5 Effect of geometric parameters of beam on the dynamic response

The effect of outer radius to the inner radius ratio of the concrete beam on the dynamic response versus time is shown in Figs. 8(a)-(d). It can be seen that with an increase in outer to inner radius ratio of the concrete beam, the structure becomes softer and the dynamic deflection of the system increases. The maximum dynamic displacements for the outer to inner radius ratio of 2, 4, 6 and 8 are 0.00053, 0.0192, 0.0407 and 0.0585, respectively. For example, with increasing the outer to inner radius ratio from 6 to 8, the maximum displacement increases up to 43.76%.

Figs. 9(a)-(d) present the effect of the beam length on the dynamic deflection of the structure versus time. It can be found that with increasing the length, the displacement of the structure increases. It is because of the reduction of the stiffness of the system when the beam becomes longer. For instance, an increase in the length of the beam from 2 m to 3 m leads to an increase in the maximum displacement of the structure up to 52.21%.

6.6 Effect of boundary conditions on dynamic response

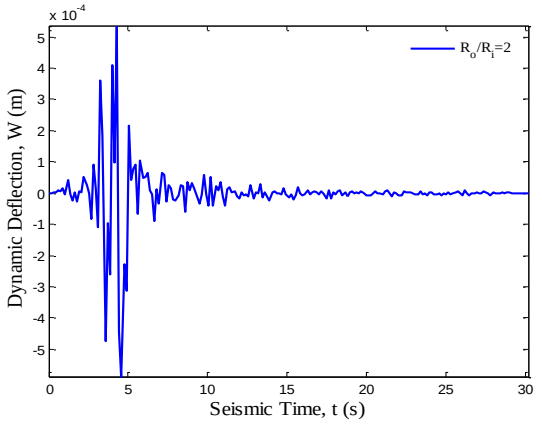

(a)

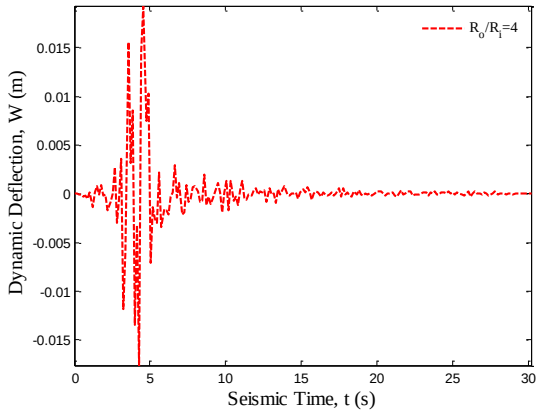

(b)

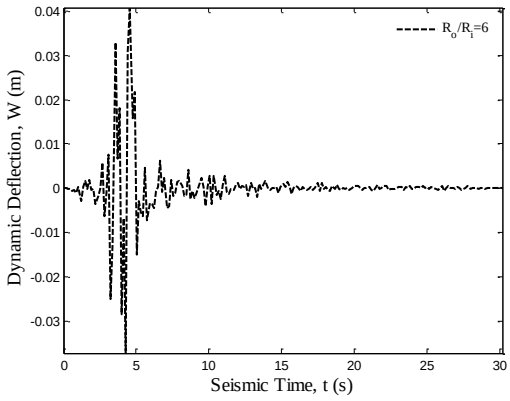

(c)

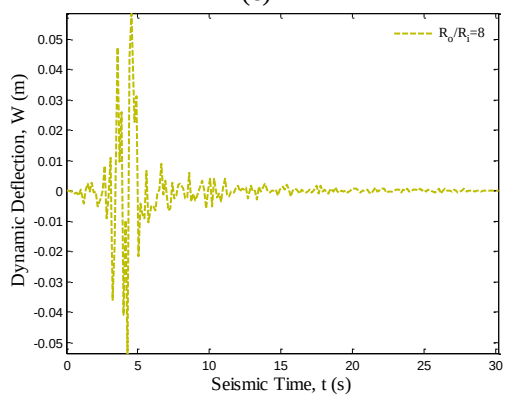

(d)

Fig. 8 The effect of outer to inner radius ratio of the concrete column on the dynamic deflection of the structure

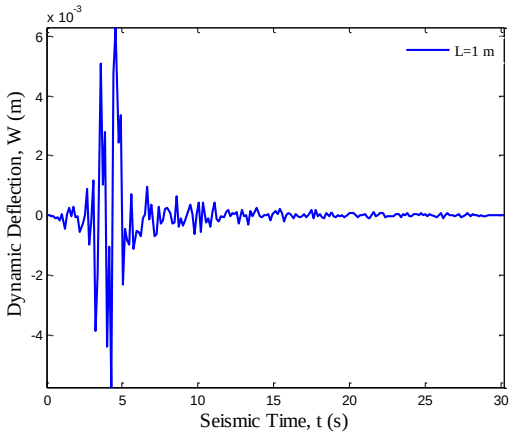

(a)

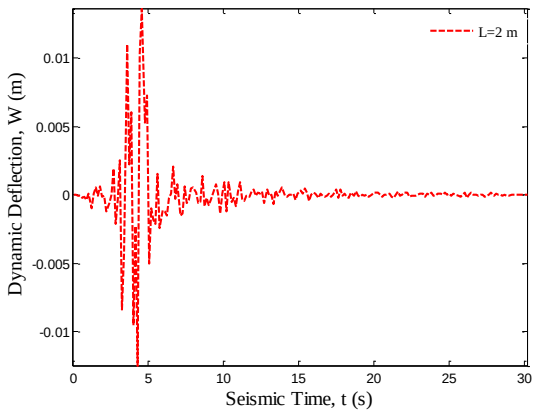

(b)

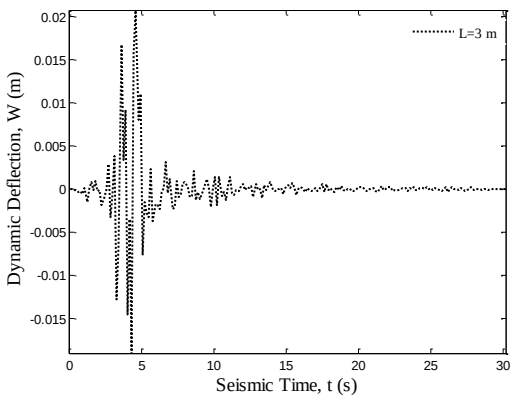

(c)

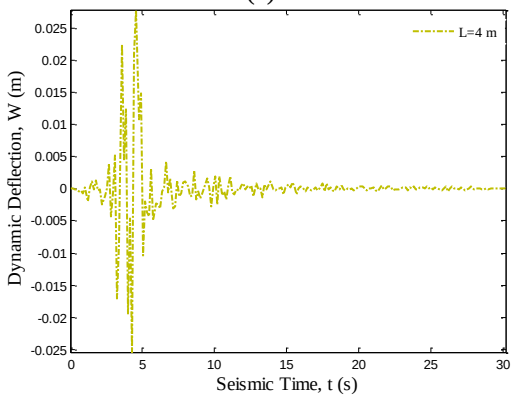

(d)

Fig. 9 The effect of column length on the dynamic deflection of the structure

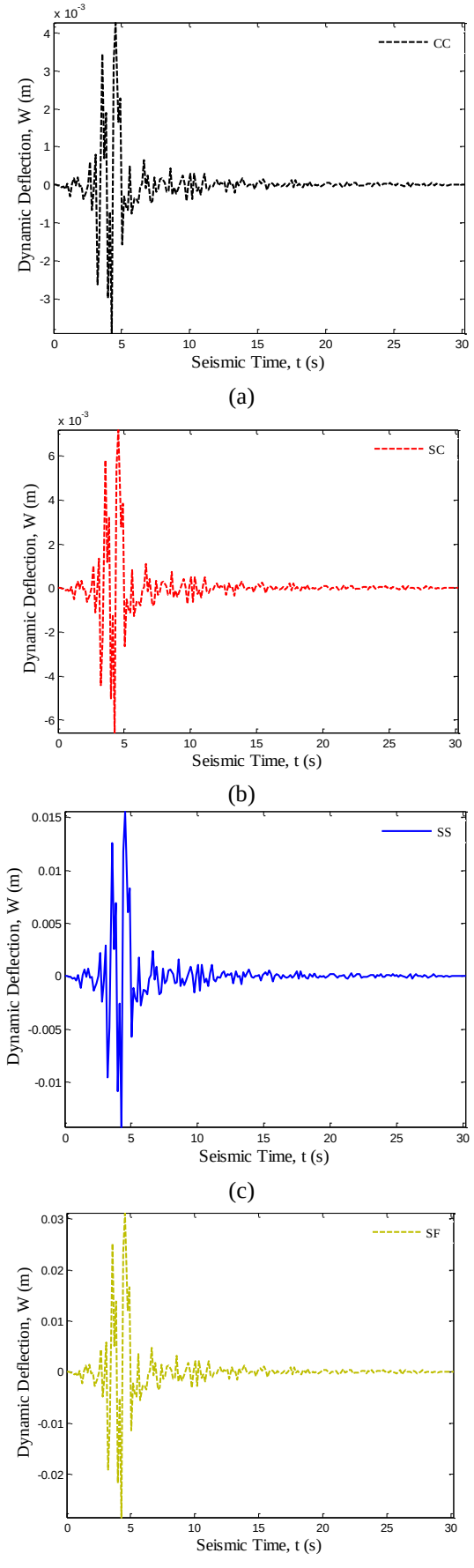

Fig. 10 The effect of boundary conditions on the dynamic deflection of the structure

Figs. 10 (a)-(d) illustrate the effect of various boundary conditions on the dynamic response versus time. Four boundary conditions including clamped-clamped, clamped-simply, simply-simply and free-simply supported are considered. The maximum dynamic deflections of the structure for clamped-clamped, clamped-simply supported, simply-simply supported and free-simply supported boundary conditions are 0.0042, 0.0072, 0.0155 and 0.0311, respectively.

As it can be observed, boundary conditions have a significant effect on the dynamic response of the system so that the structure with clamped-clamped boundary condition has the lowest displacement with respect to the other boundary conditions. It is because of the stronger constraint of the clamped boundary which gives the structure with higher stiffness.

7. Conclusions

In this research, the dynamic response of the NFRP strengthened concrete beams subjected to seismic ground excitation was studied by applying HDQM and Newmark method. The structure was modeled based on HSDBT and the agglomeration effect of nanofibers was considered using Mori-Tanaka model. By employing the nonlinear strain-displacement relations, energy formulation and Hamilton's principle, the governing equations of motion were derived. The main goal in this study was the analysis of the effect of NFRP layer, volume fraction of nanofibers, agglomeration, geometric parameters of beam and various boundary conditions on the dynamic displacement of the structure. The remarkable results can be listed as below

1. The structure without NFRP layer has a greater dynamic deflection with respect to the concrete beam covered with a NFRP layer.
2. By comparing the results, we can say that using the NFRP layer with thicknesses of 30, 60 and 90 mm decreases the maximum dynamic displacement of the structure up to 64.9%, 91.02% and 92.37%.
3. The excessive increasing of the NFRP layer (hf>60 mm) increases costs while it does not have a noticeable effect on the dynamic response of the structure.
4. Using nanofibers with volume fractions of 0.1 and 0.2, increases the stiffness of the structure and decreases the maximum displacement of 9.65% and 35.79%.
5. In the absence of the agglomeration effect (ξ=0), the maximum dynamic deflection of the structure was 0.0152 while for ξ=0.9 the maximum dynamic deflection was 0.0207. The results reveal that the existence of the agglomeration changes the maximum dynamic displacement of the structure up to 36.18%.
6. By increasing the length of the beam, the displacement of the structure increases. It was because of the decreasing of the stiffness of the system when the beam becomes longer. For instance, an increase in the length of the beam from 2 m to 3 m leads to an increase in the maximum displacement of the structure up to 52.21%.
7. Boundary conditions have a significant effect on the

dynamic response of the system so that the structure with clamped-clamped boundary condition has the lowest displacement with respect to the other boundary conditions.

8. It was also worth to mention that the volume percent of 0.34 is an optimum value since before 0.34%, the deflection is decreased while for after 0.34%, the deflection increases.

References

Alibeigloo, A. (2016), "Thermoelastic analysis of functionally graded carbon nanotube reinforced composite cylindrical panel embedded in piezoelectric sensor and actuator layers", *Compos. Part B: Eng*., **98**, 225-243.

Cao, V.V. and Ronagh, H.R. (2014), "Reducing the potential seismic damage of reinforced concrete frames using plastic hinge relocation by FRP", *Compos. Part B: Eng*., **60**, 688-696.

Changwang, Y., Jinqing, J. and Ju, Z. (2010), "Seismic behavior of steel reinforced ultra high strength concrete column and reinforced concrete beam connection", *Trans. Tianjin Univ.*, **16**(4), 309-316.

Cheng, C. and Chen, C. (2004), "Seismic behavior of steel beam and reinforced concrete column connections", *J. Construct. Steel Res*., **61**(5), 587-606.

Choi, S.W., Yousok, K. and Park, H.S. (2014), "Multi-objective seismic retrofit method for using FRP jackets in shear-critical reinforced concrete frames", *Compos. Part B: Eng*., **56**, 207-216.

Davar, A., Khalili, S.M.R. and Malekzadeh Fard, K.(2013), "Dynamic response of functionally graded circular cylindrical shells subjected to radial impulse load", *Int. J. Mech. Mater.Des*., **9**(1), 65-81.

Feng, C., Kitipornchai, S. and Yang, J. (2017a), "Nonlinear bending of polymer nanocomposite beams reinforced with non-uniformly distributed graphene platelets (GPLs)",*Compos. Part B: Eng*., **110**, 132-140.

Feng, C., Kitipornchai, S. and Yang, J. (2017b), "Nonlinear free vibration of functionally graded polymer composite beams reinforced with graphene nanoplatelets (GPLs)", *Eng. Struct*., **140**, 110-119.

Formica, G., Lacarbonara, W. and Alessi, R. (2010), "Vibrations of carbon nanotube reinforced composites", *J. Sound Vib*., **329**(10), 1875-1889.

Jafarian Arani, A. and Kolahchi, R. (2016), "Buckling analysis of embedded concrete columns armed with carbon nanotubes", *Comput. Concrete*, **17**(5), 567-578.

Ji, X., Zhang, M., Kang, H., Qian, J. and Hu, H. (2014), "Effect of cumulative seismic damage to steel tube-reinforced concrete composite columns", *Earthq. Struct*., **7**(2), 179-200.

Kolahchi, R., Rabani Bidgoli, M., Beygipoor, Gh. and Fakhar, M.H. (2013), "A nonlocal nonlinear analysis for buckling in embedded FG-SWCNT-reinforced microplates subjected to magnetic field", *J. Mech. Sci. Tech*., **29**(9), 3669-3677.

Kolahchi, R., Safari, M. and Esmailpour, M. (2016), "Dynamic stability analysis of temperature-dependent functionally graded CNT-reinforced visco-plates resting on orthotropic elastomeric medium", *Compos. Struct*., **150**, 255-265.

Lei, Z.X., Zhang, L.W., Liew, K.M. and Yu, J.L. (2014), "Dynamic stability analysis of carbon nanotube-reinforced functionally graded cylindrical panels using the element-free kp-Ritz method", *Compos. Struct*., **113**, 328-338.

Liang, X. and Parra-Montesinos, G.J. (2004), "Seismic behavior of reinforced concrete column-steel beam subassemblies and frame systems", *J. Struct. Eng*., **130**(2), 310-319.

Liew, K.M., Lei, Z.X., Yu, J.L. and Zhang, L.W. (2014), "Postbuckling of carbon nanotube-reinforced functionally graded cylindrical panels under axial compression using a meshless approach", *Comput. Method. Appl. M*., **268**, 1-17.

Liu, Z.Q., Xue, J.Y. and Zhao, H.T. (2016), "Seismic behavior of steel reinforced concrete special-shaped column-beam joints", *Earthq. Struct*., **11**(4), 665-680.

Matsunaga, H. (2007), "Vibration and buckling of cross-ply laminated composite circular cylindrical shells according to a global higher-order theory", *Int. J. Mech.Sci.*, **49**(9), 1060-1075.

Mori, T. and Tanaka, K. (1973), "Average stress in matrix and average elastic energy of materials with misfitting inclusions", *Acta Metall*., **21**(5), 571-574.

Shen, H.S. and Yang, D.Q. (2014), "Nonlinear vibration of anisotropic laminated cylindrical shells with piezoelectric fiber reinforced composite actuators", *Ocean Eng*., **80**, 36-49.

Shu, C. and Xue, H. (1997), "Explicit computations of weighting coefficients in the harmonic differential quadrature", *J. Sound Vib*., **204**(3), 549-555.

Simsek, M. (2010), "Non-linear vibration analysis of a functionally graded Timoshenko beam under action of a moving harmonic load", *Compos. Struct*., **92**(10), 2532-2546.

Simsek, M. and Reddy, J.N. (2013), "A unified higher order beam theory for buckling of a functionally graded microbeam embedded in elastic medium using modified couple stress theory", *Compos. Struct*., **101**, 47-58.

Wuite, J. and Adali, S. (2005), "Deflection and stress behaviour of nanocomposite reinforced beams using a multiscale analysis", *Compos. Struct*., **71**(3), 388-396.

CC